Intermetallics 42 (2013) 130–136

Contents lists available at SciVerse ScienceDirect

Intermetallics

journal homepage: www.elsevier.com/locate/intermet

Structural, elastic and electronic properties of new layered superconductor $HfCuGe_2$ in comparison with isostructural $HfCuSi_2$, $ZrCuGe_2$, and $ZrCuSi_2$ from first-principles calculations

I.R. Shein [a], S.L. Skornyakov [b,c], V.I. Anisimov [b,c], A.L. Ivanovskii [a,*]

[a] Institute of Solid State Chemistry, Ural Branch, Russian Academy of Sciences, 91, Pervomaiskaya Str., Ekaterinburg 620990, Russia
[b] Institute of Metal Physics, Ural Branch, Russian Academy of Sciences, GSP-170, Ekaterinburg 620041, Russia
[c] Ural Federal University, Ekaterinburg, Russia

ARTICLE INFO

Article history:
Received 29 April 2013
Accepted 6 June 2013
Available online 4 July 2013

Keywords:
A. Intermetallics
B. Electronic structure of metals and alloys
B. Elastic properties
E. *Ab-initio* calculations

ABSTRACT

Very recently, low-temperature superconductivity was discovered for the intermetallic compound $HfCuGe_2$ (*2013; Cava RJ, et al, EPL 101:67001.*), which was declared as "a non-magnetic analog of the 1111 iron pnictides". Herein, by means of the first-principles calculations, we have examined in detail the structural, elastic, and electronic properties of $HfCuGe_2$, as well as of the isostructural and isoelectronic phases $ZrCuGe_2$, $HfCuSi_2$, and $ZrCuSi_2$, which are analyzed in comparison with a set of 1111-like phases.

The obtained close similarity of the electronic factors, namely, the topologies of the near-Fermi bands, the Fermi surfaces, as well as the DOS values at the Fermi level for superconducting $HfCuGe_2$ and other examined 112 phases allowed us to assume that low-temperature superconductivity may be expected also for $ZrCuGe_2$, $HfCuSi_2$, and $ZrCuSi_2$.

1. Introduction

Superconductivity in layered (quasi-two-dimensional, quasi-2D) materials is one of the most exciting topics of modern physics and materials science. After the discovery of high-T_C superconductivity in fluorine doped LaFeAsO – so-called 1111 phase [1], tremendous attention was devoted recently to the family of layered Fe-based materials (and their Mn, Co, Ni-based analogs), which comprises several groups of quasi-2D systems (see reviews [2–11]) – from simplest binaries such as FeSe to much more complex five-component materials, among which there are so-called 42226 (or 21113) phases with nominal stoichiometry $A_4M_2Fe_2Pn_2O_6$, where M are transition metals, Pn are pnictogens, and A are alkaline earth metals, review [6]. The presence in these materials of magnetic ions determines an unconventional pairing mechanism involving spin fluctuations, as well as a set of intriguing physical properties such as charge or spin density waves (CDW or SDW), different types of magnetic ordering, coexistence of an SC phase and a CDW/SDW phase, coexistence of magnetism and superconductivity *etc.*, reviews [2–11].

Very recently, bulk superconductivity with a transition temperature T_C = 0.6 K was discovered [12] for the intermetallic compound $HfCuGe_2$, which is declared by the authors [12] as "a non-magnetic analog of the 1111 iron pnictides". Indeed, like the 1111 phases – for example, LaFeAsO, which adopts a layered tetragonal crystal structure (ZrCuSiAs type, space group P4/*nmm*, Z = 2 [12,13]) with alternating blocks [FeAs] and [LaO], the crystal structure of $HfCuGe_2$ (or, in another description, HfGeCuGe) can be viewed as alternation of blocks [CuGe] and [HfGe], which are composed of edge-shared $CuGe_4$ and $GeHf_4$ tetrahedra, respectively.

On the other hand, LaFeAsO (like other related 1111 phases) has a set of remarkable peculiarities of electronic structure and chemical bonding, namely: (i) the electronic bands in the window around the Fermi level (E_F) are formed mainly by the states of blocks [FeAs] and play the main role in superconductivity; (ii) the oxide blocks [LaO] are insulating and serve as "charge reservoirs"; and (iii) the inter-atomic bonding is highly anisotropic and includes ionic, covalent, and metallic contributions inside blocks [FeAs], mixed covalent-ionic bonds inside blocks [LaO], whereas the inter-block bonding is of the ionic type, see Refs. [3,8]. At the same time, as far as we know, there are no available data on the electronic structure of the newly discovered superconducting $HfCuGe_2$.

In view of these circumstances, in this paper a first-principle study was performed in order to get an insight into the basic structural, elastic, and electronic properties of $HfCuGe_2$ and three known isostructural and isoelectronic phases [13]: $ZrCuGe_2$,

* Corresponding author.
E-mail address: ivanovskii@ihim.uran.ru (A.L. Ivanovskii).

0966-9795/$ – see front matter © 2013 Elsevier Ltd. All rights reserved.
http://dx.doi.org/10.1016/j.intermet.2013.06.001

$HfCuSi_2$, and $ZrCuSi_2$ (112 phases). Our characterization of these 112 phases covers the optimized structural parameters, the main elastic parameters (elastic constants (C_{ij}), bulk (B), shear (G), and Young's moduli (Y), Poisson's ratio (ν), anisotropy indexes, and Pugh's criterion (G/B ratio)), as well as electronic bands, Fermi surfaces, and density of electronic states, which are analyzed in comparison with some of the aforementioned 1111 phases.

2. Models and computational aspects

The examined 112 phases: $HfCuGe_2$, $ZrCuGe_2$, $HfCuSi_2$, and $ZrCuSi_2$ are isostructural and adopt a layered tetragonal crystal structure, space group P4/*nmm*, as depicted in Fig. 1. The Wyckoff positions of atoms are (Hf,Zr): 2*c* (¼,¼,z_M); Cu: 2*b* (¼,¾ ,½); (Ge_1,Si_1): 2*a* (¼,¾ ,0), and (Ge_2,Si_2): 2*c* (¼,¼,z_x); here, z_M and z_x are the so-called internal coordinates [13]. The structures are defined by the lattice parameters a and c and the internal parameters z_M and z_x.

Our calculations of the above materials were performed using two complementary DFT-based codes.

Firstly, the structural and electronic properties of the aforementioned systems were examined by means of the full-potential method with mixed basis APW + lo (LAPW) implemented in the WIEN2k suite of programs [14]. The generalized gradient correction (GGA) to exchange-correlation potential of Perdew, Burke, and Ernzerhof [15] was used. The basis set inside each MT sphere was split into core and valence subsets. The core states were treated within the spherical part of the potential only, and were assumed to have a spherically symmetric charge density confined within MT spheres. The valence part was treated with the potential expanded into spherical harmonics to $l = 4$. The valence wave functions inside the spheres were expanded to $l = 10$. The plane-wave expansion with $R_{MT} \times K_{MAx}$ was equal to 7.0, and k sampling with a $16 \times 16 \times 5$ k-point mesh in the full Brillouin zone was used. The MT sphere radii were chosen to be 2.1 a.u. for Ge and Si and 2.4 a.u. for Cu, Zr, and Hf. The Blöchl's modified tetrahedron method [16] was employed for the densities of states (DOSs) calculations.

Secondly, for the calculations of the elastic parameters we employed the Vienna *ab initio* simulation package (VASP) in the projector augmented waves (PAW) formalism [17,18]. Exchange and correlation were also described in the form of GGA [15]. The kinetic energy cutoff of 500 eV and a k-mesh of $16 \times 16 \times 5$ were used. The geometry optimization was performed with the force cutoff of 1 meV/Å. These two DFT-based codes are complementary and allow us to perform a complete investigation of the declared properties of the above materials.

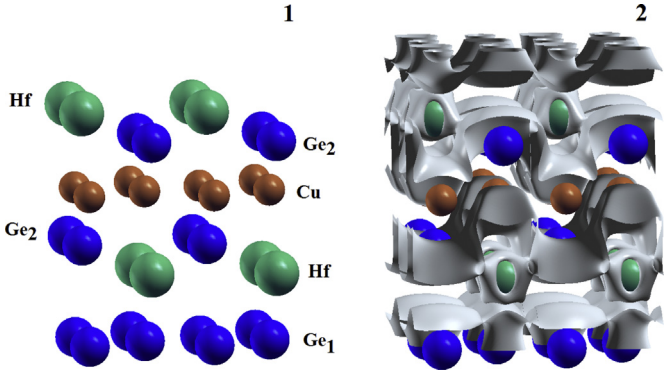

Fig. 1. Fragment of the atomic structure of the 112 phase $HfCuGe_2$ (non-equivalent germanium atoms, Ge_1 and Ge_2, are labeled) and the charge density map illustrating the formation of a 3D-like system of inter-atomic bonds in this material.

3. Results and discussion

3.1. Structural properties

As the first step, the equilibrium lattice constants (a and c) for $HfCuGe_2$, $ZrCuGe_2$, $HfCuSi_2$, and $ZrCuSi_2$ phases were calculated with full structural optimization including internal parameters z_M and z_x. The results obtained are listed in Table 1 in comparison with experimental data [13]. Firstly, our data are in reasonable agreement with the available experiments. Secondly, as a result of substitutions of Zr for Hf and of Si for Ge, the lattice parameters a and c increase in the sequences $HfCuGe_2 \rightarrow ZrCuGe_2$ and $HfCuSi_2 \rightarrow ZrCuSi_2$ and decrease in the sequences $HfCuGe_2 \rightarrow HfCuSi_2$ and $ZrCuGe_2 \rightarrow ZrCuSi_2$. This trend can be easily explained by considering the atomic radii of Hf (1.59 Å) *versus* Zr (1.60 Å) and Ge (1.39 Å) *versus* Si (1.34 Å). Next, our results demonstrate that replacements of the atoms (Hf ↔ Zr or Ge ↔ Si) lead to *anisotropic deformations* of the crystal structure. So, in the sequence $HfCuGe_2 \rightarrow ZrCuGe_2$, the parameter a increases by $(a^{HfCuGe2} - a^{HfCuSi2})\, a^{HfCuGe2} \sim 2.6\%$, whereas the parameter c increases only by $(c^{HfCuGe2} - c^{HfCuSi2})/c^{HfCuGe2} \sim 1.3\%$. This effect should be attributed to anisotropy of inter-atomic bonds: inside atomic sheets *versus* inter-sheet interactions.

Finally, it is interesting to compare the structural peculiarities of the discussed 112 phases with those of some 1111-like materials. For this purpose we used the so-called buckling parameter [19]: $q = (1 - z_x)/z_M$, which reflects the tetragonal distortions within blocks (*MX*) and (CuAs), and the values of c/a.

In Fig. 2, the so-called structural map (c/a *versus* q) is depicted for various 1111-like phases calculated earlier by the authors [20–26] within the same FLAPW method. We see that 1111 phases are divided into three separate groups I–III. Here, all oxygen-containing phases, including the metallic-like parent phases of Fe-based superconductors (LaFeAsO, LaFePO) or *p*-type transparent semiconductors like *Ln*Cu*Ch*O, belong to groups I and II with high values of $q > 2$, *i.e.* with quite high separation of building blocks. On the contrary, for the oxygen-free *M*Cu*X*As phases (such as HfCuGeAs or ZrCuSiAs, Fig. 2) the buckling parameters are much smaller, $q < 1.5$, reflecting the expansion of blocks along the c axis, which, in turn, promotes the formation of directional bonds between the adjacent blocks. Indeed, the analysis of the inter-atomic bonding in the 1111 phases of group III reveals [25] that they may be viewed as 3D-like systems owing to the presence of strong covalent bonds between the adjacent blocks (*MX*)/(CuAs) together with directional bonds inside each block.

The examined 112 phases also adopt quite small buckling parameters ($q \sim 1.35$–1.40, Fig. 2), therefore already from the structural data we can expect that these materials will behave as 3D-like systems, see also below.

3.2. Elastic properties

At first, six independent elastic constants (C_{ij}; namely C_{11}, C_{12}, C_{13}, C_{33}, C_{44}, and C_{66}) for the tetragonal 112 phases were evaluated

Table 1
Lattice parameters (a and c, in Å) and internal coordinates (z_M and z_x) for $HfCuGe_2$, $HfCuSi_2$, $ZrCuGe_2$ and $ZrCuSi_2$ as obtained within FLAPW–GGA.

Phase	$HfCuGe_2$	$HfCuSi_2$	$ZrCuGe_2$	$ZrCuSi_2$
a	3.756 (3.745)[a]	3.658 (3.692)	3.778 (3.787)	3.681 (3.719)
c	8.967 (9.020)	8.850 (8.949)	9.075 (9.120)	8.980 (9.010)
c/a	2.387 (2.409)	2.419 (2.424)	2.402 (2.408)	2.440 (2.423)
$z_{Hf(Zr)}$	0.237 (0.246)	0.235 (0.259)	0.238 (0.246)	0.236 (0.259)
$z_{Ge(Si)}$	0.678 (0.676)	0.674 (0.689)	0.675 (0.676)	0.670 (0.689)

[a] Available experimental data, Ref. [13], are given in parentheses.

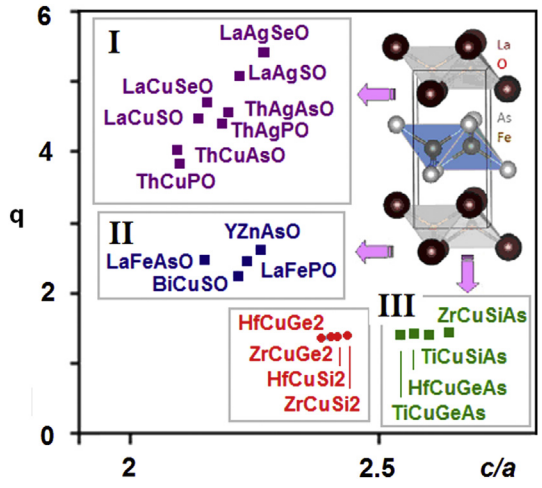

Fig. 2. Structural map for the examined 112 phases in comparison with various groups of quaternary tetragonal 1111 phases (I–III, see text) as obtained from optimized structural data within FLAPW calculations [20–26]. *Inset*: Fragment of the atomic structure of the 1111 phase LaFeAsO [12].

by calculating the stress tensors on different deformations applied to the equilibrium lattice of the tetragonal unit cell, whereupon the dependence between the resulting energy change and the deformation was determined.

The data obtained (Table 2) reveal that all C_{ij} are positive and satisfy the well-known criterion [27] for tetragonal crystals: $C_{11} > 0$, $C_{33} > 0$, $C_{44} > 0$, $C_{66} > 0$, $(C_{11} - C_{12}) > 0$, $(C_{11} + C_{33} - 2C_{13}) > 0$, and $\{2(C_{11} + C_{12}) + C_{33} + 4C_{13}\} > 0$. This indicates that all the examined 122 phases are mechanically stable.

Secondly, using the constants C_{ij}, we calculated monocrystalline bulk moduli (B) and shear moduli (G) in Voigt (V) [28] and Reuss (R) [29] approximations as:

$$B_V = 1/9\{2(C_{11} + C_{12}) + C_{33} + 4C_{13}\};$$

$$G_V = 1/30\{M + 3C_{11} - 3C_{12} + 12C_{44} + 6C_{66}\};$$

$$B_R = C^2/M;$$

$$G_R = 15\left\{18B_V/C^2 + 6/(C_{11} - C_{12}) + 6/C_{44} + 3/C_{66}\right\}^{-1};$$

where $C^2 = C_{33}(C_{11} + C_{12}) - 2C_{13}^2$ and $M = C_{11} + C_{12} + 2C_{33} - 4C_{13}$.

We evaluated also the corresponding parameters for polycrystalline *M*Cu*X*As species, *i.e.* for materials in the form of aggregated mixtures of microcrystallites with random orientation. For this purpose we utilized the Voigt–Reuss–Hill (VRH) approximation [30]. In this approach, the actual effective moduli (B and G) for polycrystals are approximated by the arithmetic mean of the two above mentioned limits – Voigt and Reuss, which further allowed us to obtain the average Young's moduli (Y) and the Poisson's ratio (ν) as:

$$Y = 9B/\{1 + (3B/G)\},$$

$$\nu = (3B - 2G)/2(3B + G)$$

These parameters are presented in Table 2 and allow us to make the following conclusions:

- The obtained values show that the highest bulk modulus B (which represents the resistance to volume change) is adopted by $HfCuGe_2$, whereas the highest shear modulus (which represents the resistance to shear deformation against external forces) is found for $HfCuSi_2$. Note that in general these values for the examined 112 phases are comparable with the bulk and shear moduli of their nearest 1111-like analogs: ZrCuSiAs, HfCuSiAs, ZrCuGeAs, and HfCuGeAs, see Fig. 3. Besides, as $B > G$, the parameter limiting the mechanical stability of these materials is the shear modulus G.
- Brittle/ductile behavior is one of important mechanical characteristics of materials, which is closely related to their reversible compressive deformation and fracture ability. One of the most widely used malleability measures of materials is the Pugh's criterion (G/B ratio) [31]. As is known, if $G/B < 0.5$, a material behaves in a ductile manner, and *vice versa*, if $G/B > 0.5$, a material demonstrates brittleness. According to this indicator (Table 2), the examined 112 phases will behave as brittle materials, though $HfCuGe_2$ ($G/B = 0.54$) and $ZrCuGe_2$ ($G/B = 0.58$) lie near the border of brittleness. An additional indicator of brittle/ductile behavior follows from the Poisson's ratio (ν); for the 112 phases, the calculated values of ν (Table 2)

Table 2
Calculated elastic parameters for 112 phases $HfCuGe_2$, $HfCuSi_2$, $ZrCuGe_2$ and $ZrCuSi_2$: elastic constants (C_{ij}, in GPa), bulk moduli (B, in GPa), compressibility (β, in GPa^{-1}), shear moduli (G, in GPa), Pugh's indicator (G/B), Young's moduli (Y, in GPa), Poisson's ratio (ν), and indexes of elastic anisotropy (A_B, A_G, in %, and A^U) as obtained within VASP.

Phase	$HfCuGe_2$	$HfCuSi_2$	$ZrCuGe_2$	$ZrCuSi_2$
C_{11}	222.6	240.8	216.3	205.3
C_{33}	197.7	180.1	192.5	155.1
C_{44}	75.5	111.8	79.1	111.2
C_{66}	100.8	122.9	99.4	89.1
C_{12}	103.4	108.1	90.4	66.6
C_{13}	99.0	85.8	93.0	54.0
B_V	138.4	135.7	130.9	101.7
B_R	137.8	131.5	130.6	99.3
B	138.1	133.6	130.7	100.5
β	0.00724	0.00749	0.00765	0.00995
G_V	75.6	94.8	77.4	88.4
G_R	73.1	92.4	74.8	85.9
G	74.4	93.6	76.1	87.2
G/B	0.54	0.70	0.58	0.88
Y	189.1	227.6	191.1	202.8
ν	0.272	0.216	0.256	0.164
A_B	0.22	1.60	1.15	1.19
A_G	1.68	0.96	1.71	1.43
A^U	0.17	0.16	0.17	0.17

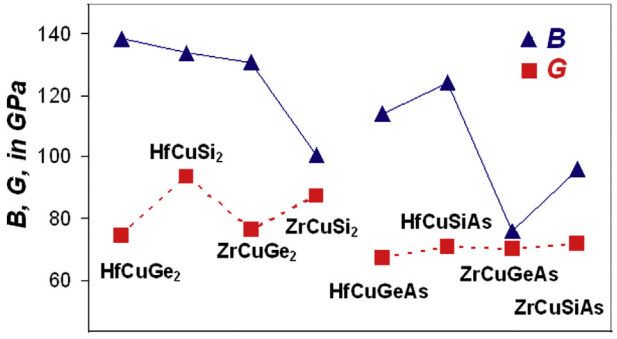

Fig. 3. Elastic parameters: bulk (B) and shear (G) moduli for the examined 112 phases in comparison with those of their nearest 1111-like analogs: ZrCuSiAs, HfCuSiAs, ZrCuGeAs, and HfCuGeAs [25].

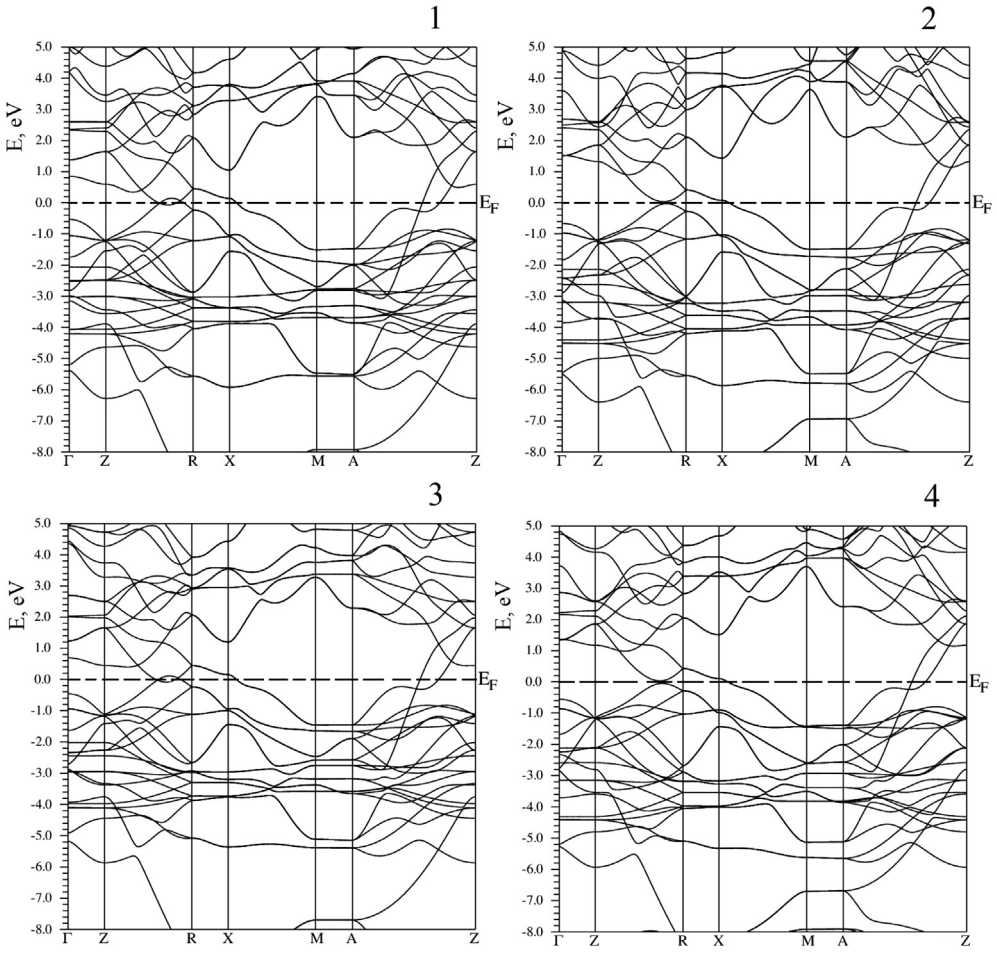

Fig. 4. Band structures of $HfCuGe_2$ (1), $HfCuSi_2$ (2), $ZrCuGe_2$ (3), and $ZrCuSi_2$ (4).

are smaller than $\nu \sim 0.33$, which is typical of ductile metallic materials [32].

- The Young's modulus (Y) of materials is defined as a ratio of linear stress to linear strain, which tells about their stiffness. The average Young's moduli for 112 phases (Table 2) were found to be $Y \sim 190$–230 GPa; thus, these materials will show a rather moderate stiffness.
- Elastic anisotropy of crystals reflects a different character of bonding in different directions and has an important implication since it correlates with the possibility to induce microcracks in materials. There are different ways to evaluate the elastic anisotropy of crystals, see review [33]. Among them, one way implies estimation of elastic anisotropy (in %) in compressibility (A_B) and shear (A_G) using a model [34] for polycrystalline materials:

$$A_B = (B_V - B_R)/(B_V + B_R),$$

$$A_G = (G_V - G_R)/(G_V + G_R)$$

Additionally, the so-called universal anisotropy index [35] was used, which is defined as:

$$A^U = 5G_V/G_R + B_V/B_R - 6.$$

For isotropic crystals $A^U = 0$; deviations of A^U from zero define the extent of crystal anisotropy. The calculated data (Table 2) indicate that all the 112 phases exhibit quite small and comparable elastic anisotropy in shear and in compressibility.

- Finally, the calculated elastic parameters enable us to evaluate in a simplified manner the hardness of materials. Note that this macroscopic parameter is usually characterized experimentally by indentation, and therefore it depends strongly on plastic (irreversible) deformation, review [33]. On the other hand, a set of empirical relationships between Vickers hardness (H_V) and elastic moduli was proposed [33,36]. So, according to Teter [37], the polycrystalline shear modulus can be used as a predictor of hardness, and the value of hardness can be estimated as: $H_V = 0.1769G - 2.899$. Related linear relationships were proposed recently [38]: $H_V = 0.1475G$ and $H_V = 0.0607Y$. Our numerical estimations reveal that the examined 122 phases will exhibit moderate hardness (of about 9–14 GPa), which is comparable with H_V for their nearest 1111-like analogs: ZrCuSiAs, HfCuSiAs, ZrCuGeAs, and HfCuGeAs [25].

3.3. Electronic properties and chemical bonding

The electronic bands and total and partial densities of states (DOSs) of the 112 phases are depicted in Figs. 4 and 5, respectively, and are similar for all four isoelectronic and isostructural systems. The general view on the electronic structure of these phases can be obtained from their DOSs depicted in Fig. 5. The most intense DOSs peaks lie around −3.5 eV below the Fermi level (E_F) and are formed

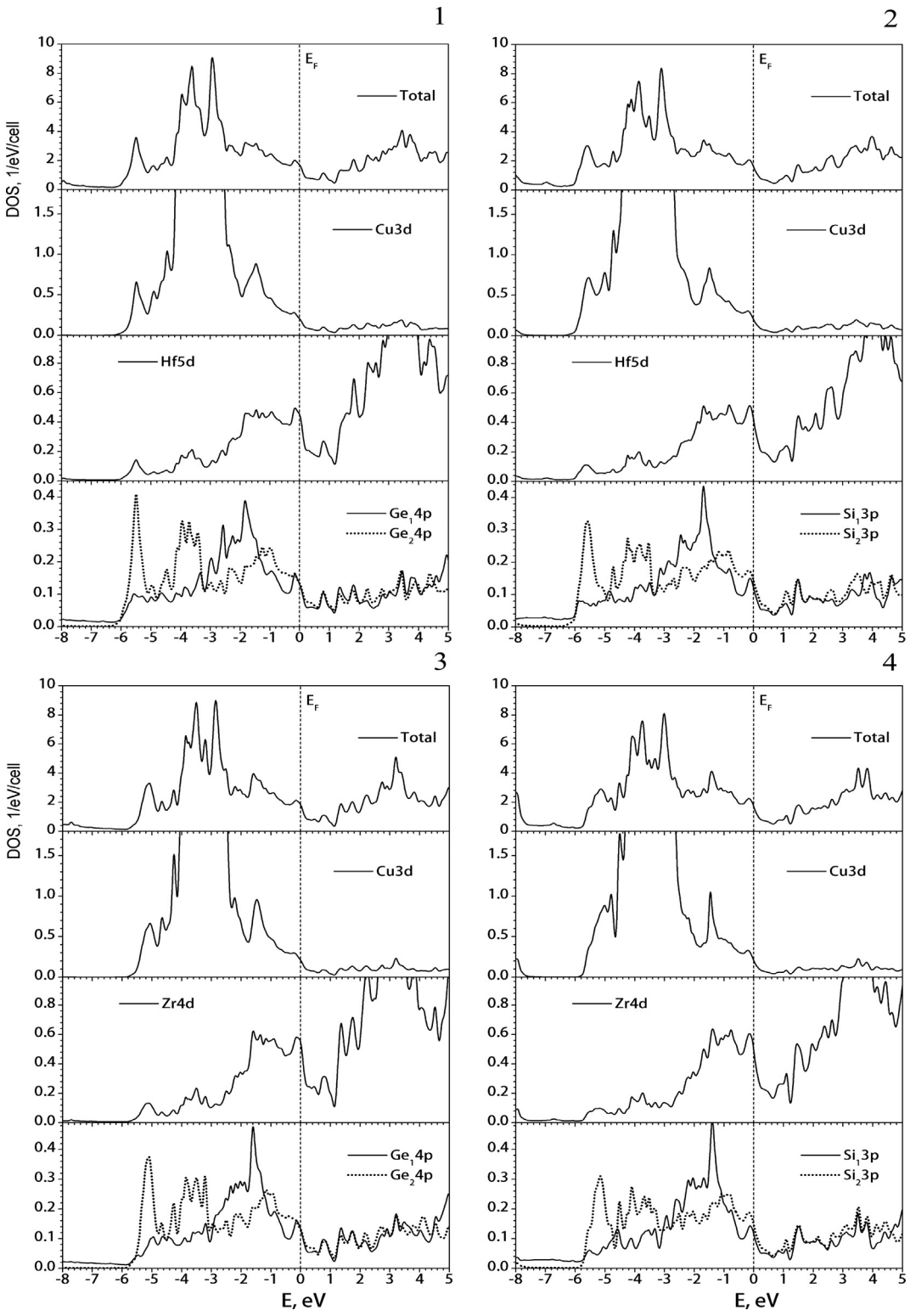

Fig. 5. Density of states for $HfCuGe_2$ (1), $HfCuSi_2$ (2), $ZrCuGe_2$ (3), and $ZrCuSi_2$ (4).

predominantly by Cu 3*d* states, whereas the Hf 5*d* (Zr 4*d*) states are located mainly in the interval from −3 eV to E_F. In turn, the Ge(Si) states are distributed over the valence band.

Since electrons near the Fermi level are involved in the formation of the superconducting state, it is important to understand their nature. The total and atomic decomposed partial DOSs at the Fermi level, $N(E_F)$, are shown in Table 3. It is seen that for the superconducting $HfCuGe_2$ comparable contributions to $N(E_F)$ come from the Hf 5*d*, Cu 3*d*, and Ge states. Thus, we cannot identify a building block, which will be responsible for the metallic-like (and superconducting) properties of this material – unlike 1111 phases such as LaFeAsO, where the near-Fermi bands are formed exclusively by the Fe 3*d* states from [FeAs] blocks, see Refs. [3–8].

Table 3
Total, atomic- and orbital-resolved densities of states at the Fermi level for $HfCuGe_2$, $HfCuSi_2$, $ZrCuGe_2$, and $ZrCuSi_2$.

Phase	$HfCuGe_2$	$HfCuSi_2$	$ZrCuGe_2$	$ZrCuSi_2$
$N(E_F)^{total}$	1.71	1.59	1.83	1.71
Hf(Zr) *d*	0.45	0.42	0.54	0.49
d_{z2}	0.16	0.12	0.19	0.14
d_{xy}	0.09	0.11	0.11	0.15
d_{x2+y2}	0.04	0.03	0.05	0.02
d_{xz+yz}	0.16	0.16	0.19	0.18
Cu 3*d*	0.21	0.20	0.21	0.21
$3d_{z2}$	0.07	0.07	0.07	0.08
$3d_{xy}$	0.04	0.03	0.03	0.03
$3d_{x2+y2}$	0.03	0.04	0.04	0.04
$3d_{xz+yz}$	0.07	0.06	0.07	0.06
$Ge_1(Si_1)$ *p*	0.13	0.12	0.13	0.12
p_z	0.04	0.04	0.04	0.04
p_{x+y}	0.09	0.08	0.09	0.08
$Ge_2(Si_2)$ *p*	0.13	0.14	0.13	0.15
p_z	0.05	0.05	0.05	0.05
p_{x+y}	0.08	0.09	0.08	0.10

Besides, the Fermi surfaces (FSs) topology of $HfCuGe_2$ (Fig. 6) and LaFeAsO becomes quite different. The FS for $HfCuGe_2$ adopts a complicated multi-sheet type and contains a set of intersected hole-type and electron-type pockets, whereas the FS of LaFeAsO is much more simple and includes a set of disconnected tube-like sheets along the *z* direction, see Refs. [3,8].

Since the topologies of the near-Fermi bands and the Fermi surfaces and the DOSs values at the Fermi level, $N(E_F)$, for the superconducting phase $HfCuGe_2$ and for the other examined 112 phases are very similar (Table 3, Figs. 3–6), low-temperature superconductivity can be expected also for $ZrCuGe_2$, $HfCuSi_2$, and $ZrCuSi_2$.

Finally, as can be seen in Fig. 4, where the partial DOSs for 112 phases are depicted, the Ge(Si) orbitals are hybridized with Hf(Zr) and Cu states, forming Ge(Si)–Hf(Zr) and Ge(Si)–Cu bonds. In turn, these interactions form a system of 3D-like bonds, and this situation is clearly visible in Fig. 1, where the valence charge density map for $HfCuGe_2$ is given as an example. Again, this 3D-like type of interatomic interactions in 112 phases differs considerably from the bonding picture in LaFeAsO, where a 2D-like system of the bonds takes place, see Refs. [3,8].

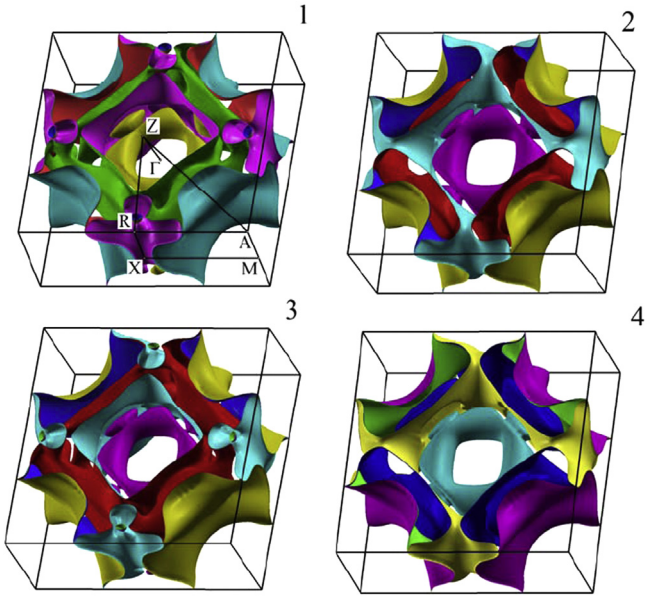

Fig. 6. Fermi surfaces of $HfCuGe_2$ (1), $HfCuSi_2$ (2), $ZrCuGe_2$ (3), and $ZrCuSi_2$ (4).

4. Conclusions

In summary, by means of the first-principles calculations, we studied in detail the structural, elastic, and electronic properties for a newly discovered [12] low-temperature superconductor – the intermetallic compound $HfCuGe_2$ (which is declared by the authors [12] as "a non-magnetic analog of the 1111 iron pnictides") and for the isostructural and isoelectronic phases $ZrCuGe_2$, $HfCuSi_2$, and $ZrCuSi_2$.

Our main findings are as follows:

(i) The examined 112 phases will behave as brittle materials with rather moderate stiffness exhibiting quite small and comparable elastic anisotropy in shear and compressibility;
(ii) The near-Fermi electronic bands, which are responsible for the metallic-like behavior of these materials and which will be involved in the formation of superconducting state, include comparable contributions from the Hf (Zr)*d*, Cu 3*d*, and Ge(Si) states; therefore we cannot identify a building block, which will be responsible for the aforementioned properties of 112 phases – unlike the 1111 phases such as LaFeAsO, where the near-Fermi bands are formed exclusively by the Fe 3*d* states from [FeAs] blocks.
(iii) Our calculations indicate that also the topology of the Fermi surfaces of the 112 phases and LaFeAsO becomes different: the FS for 122 materials adopts quite a complicated multi-sheet type and contains a set of intersected hole-type and electron-type pockets, whereas the FS of LaFeAsO is much more simple and includes a set of disconnected tube-like sheets along *z* direction.
(vi) Our analysis reveals that for the 112 phases the inter-atomic bonding is of a 3D-like type involving Ge(Si)–Hf(Zr) and Ge(Si)–Cu bonds – unlike the bonding picture for LaFeAsO, where a 2D-like system of bonds takes place.
(v) Finally, the obtained close similarity of the topologies of the near-Fermi bands, the Fermi surfaces, and the DOSs values at the Fermi level for the superconducting $HfCuGe_2$ and the other examined 112 phases allowed us to speculate that low-temperature superconductivity may be expected also for $ZrCuGe_2$, $HfCuSi_2$, and $ZrCuSi_2$.

Acknowledgments

This work is supported by Program of basic researches of Ural Branch, Russian Academy of Sciences (grant No. 12-T-3-1003) and Russian Foundation of Basis Researches (grants No. 11-03-00052-a, 12-02-91371-CT-a, and 13-02-00050), The Found of the President of RF for the support of Science Shools NSH-6172.2012.2, and the grant of the Ministry of Education and Science of Russia No. 14.A18.21.0076.

References

[1] Kamihara Y, Watanabe T, Hirano M, Hosono H. J Am Chem Soc 2008;130:3296.
[2] Pöttgen R, Johrendt D. Z Naturforsch B 2008;63:1135.
[3] Ivanovskii AL. Phys – Uspekhi 2008;51:1229.
[4] Ren ZA, Zhao ZX. Adv Mater 2009;21:4584.
[5] Paglione J, Greene RL. Nat Phys 2010;6:645.
[6] Ivanovskii AL. Russ Chem Rev 2010;79:1.
[7] Aswathy PM, Anooja JB, Sarun PM, Syamaprasad U. Supercond Sci Technol 2010;23:073001.
[8] Johnson DC. Adv Phys 2010;59:803.
[9] Ivanovskii AL. Physica C 2011;471:409.
[10] Johrendt D. J Mater Chem 2011;21:13726.

[11] Johrendt D, Hosono H, Hoffmann RD, Pöttgen R. Z Kristallogr 2011;226:435.
[12] Schoop L, Hirai D, Felser C, Cava RJ. EPL 2013;101:67001.
[13] Andrukhiv L, Lysenko L, Yarmolyuk Y, Gladyshevskii E. Dopov Akad Nauk Ukr RSR Ser A Fiz-Tekh Mat Nauki 1975;7:645.
[14] Blaha P, Schwarz K, Madsen GKH, Kvasnicka D, Luitz J. WIEN2k, an augmented plane wave plus local orbitals program for calculating crystal properties. Vienna: Vienna University of Technology; 2001.
[15] Perdew JP, Burke S, Ernzerhof M. Phys Rev Lett 1996;77:3865.
[16] Blöchl PE, Jepsen O, Anderson OK. Phys Rev B 1994;49:16223.
[17] Kresse G, Joubert D. Phys Rev B 1994;59:1758.
[18] Kresse G, Furthmuller J. Phys Rev B 1996;54:11169.
[19] Baergen AM, Blanchard PER, Stoyko SS, Mar A. Z Anorg Allg Chem 2011;637:2007.
[20] Shein IR, Ivanovskii AL. Physica C 2009;469:15.
[21] Bannikov VV, Shein IR, Ivanovskii AL. Mater Chem Phys 2009;116:129.
[22] Bannikov VV, Shein IR, Ivanovskii AL. Comput Mater Sci 2011;50:2736.
[23] Shein IR, Ivanovskii AL. Solid State Commun 2010;150:640.
[24] Bannikov VV, Shein IR, Ivanovskii AL. Solid State Sci 2012;14:89.
[25] Bannikov VV, Shein IR, Ivanovskii AL. J Allows Comp 2012;533:71.
[26] Shein IR, Bannikov VV, Ivanovskii AL. J Mater Sci 2012;47:6741.
[27] Born M, Huang K. Dynamical theory of crystal lattices. Oxford: Clarendon; 1956.
[28] Voigt W. Lehrbuch der Kristallphysik. Leipzig: Teubner; 1928.
[29] Reuss A. Z Angew Math Mech 1929;9:49.
[30] Hill RH. Proc Phys Soc London A 1952;65:349.
[31] Pugh SF. Philos Mag 1953;45:823.
[32] Haines J, Leger JM, Bocquillon G. Annu Rev Mater Res 2001;31:1.
[33] Ivanovskii AL. Progr Mater Sci 2012;57:184.
[34] Chung H, Buessem WR. Vahldiek FW, Mersol SA, editors. Anisotropy in single crystal refractory compound. Plenum; 1968.
[35] Ranganathan SI, Ostoja-Starzewshi M. Phys Rev Lett 2008;101:055504.
[36] Ivanovskii AL. Int J Refract Metals Hard Mater 2013;36:179.
[37] Teter D. MRS Bull 1998;23:22.
[38] Jiang J, Zhao J, Jiang X. Comput Mater Sci 2011;50:2287.